Available online at www.sciencedirect.com
ScienceDirect
Journal of Physics and Chemistry of Solids 69 (2008) 1632–1640
JOURNAL OF PHYSICS AND CHEMISTRY OF SOLIDS
www.elsevier.com/locate/jpcs

Structure and dehydration of the pyrochlore system $NaW_{2-y}Mo_yO_{6+\delta}\cdot nH_{2-z}O$ between 10 and 675 K

Gordon J. Thorogood[a,b,*], Brendan J. Kennedy[b], Vittorio Luca[a], Mark Blackford[a], Samantha K. van de Geest[a], Kim S. Finnie[a], John V. Hanna[a], Kevin J. Pike[a]

[a]*Institute of Materials and Engineering Science, Australian Nuclear Science and Technology Organisation, Private Mail Bag 1, Menai, NSW 2234, Australia*
[b]*School of Chemistry, The University of Sydney, Sydney, NSW 2006, Australia*

Received 18 May 2007; received in revised form 3 December 2007; accepted 3 December 2007

Abstract

The temperature dependence of the structure of the pyrochlore $NaW_{2-y}Mo_yO_{6+\delta}\cdot nH_{2-z}O$ has been investigated using a variety of diffraction and spectroscopic methods. The positions of OH^-/H_2O molecules in the structure have been determined. Increases in temperature induce small lattice parameter changes, which are thought to result from movement of the H_2O molecules in the pyrochlore lattice.

Keywords: C. X-ray diffraction; D. NMR; C. IR spectroscopy

1. Introduction

There has been significant recent interest in the use of ion exchangers for the separation of radioactive Cs and Sr from intermediate level liquid waste (ILLW) streams. Recent focus has been on hydrothermally prepared microcrystalline hexagonal tungsten bronzes (HTB) and related materials such as pyrochlores, since these show high selectivity for these elements. Recently, we observed that the addition of small amounts of Mo to HTB significantly enhances their ion-exchange properties [1,2], this is also the case for the pyrochlore form.

The $A_2B_2O_7$ pyrochlore structure was first reported by von Gaertner [3] and pyrochlore oxides have been found to exhibit a rich variety of physical and chemical properties [4]. For example, Barnes et al. [5] showed a link between pressure-induced cation migration and volume expansion in defect pyrochlores. The use of pyrochlores as ion exchangers to remove Sr-90 and Cs-137 from liquid waste streams was first investigated by Möller et al. [6–10]. Recently, the removal of these species by titanosilicates has been investigated by various authors [11–13]. One aspect of the pyrochlore system not studied by Möller [14], although mentioned as important, was to establish the role of the structural water in the ion-exchange process. The presence of H_2O in natural and synthetic pyrochlores has been long known [15].

It is well established that the pyrochlore A-type cation, in hydrothermally prepared pyrochlores, can exchange with other cations in aqueous solutions [10]. The extent of ordering of the A-type cation and water molecules in the hydrothermally produced pyrochlores has not been established nor has the effect of thermal annealing been reported. The precise A–H_2O arrangement is likely to influence the ion-exchange properties of the pyrochlores and thermal treatment may be a method to optimize this.

The defect pyrochlore structure has a cubic symmetry (space group $Fd\bar{3}m$) and a stoichiometry of $A_{2-\delta}B_2X_6X'_{1-\delta}$ or if $\delta = 1$ AB_2X_6, where A is a large low valence cation and B is a smaller cation which is capable of octahedral coordination (e.g., Ti^{4+}, Zr^{4+}, W^{6+}, Sb^{6+}). The X anion site is usually occupied by O^{2-}, however, the X′ site can

*Corresponding author at: Institute of Materials and Engineering Science, Australian Nuclear Science and Technology Organisation, Private Mail Bag 1, Menai, NSW 2234, Australia. Tel.: +61 297173183; fax: +61 295437179.
E-mail address: gjt@ansto.gov.au (G.J. Thorogood).

0022-3697/$ - see front matter
doi:10.1016/j.jpcs.2007.12.008

also be occupied by anions such as OH^- or F^-. The pyrochlore structure is built on corner sharing BX_6 octahedra [16] that form a framework of tunnels with cavities of tetrahedral symmetry at the tunnel intersections. The opening to these cavities form puckered hexagons of O atoms [17]. In the ideal pyrochlore structure, the A-type cations are located on the 16d Wycoff site (0.5, 0.5, 0.5) and the X′ anion is normally located at the 8b sites (3/8, 3/8, 3/8).

Pyrochlores, when produced hydrothermally, tend to have bound water within the structure and it is reported that the H_2O molecules are located within the B_2O_6 tunnels and can occupy 8b, 16d or 32e positions. In a structural study of antimonic acid, Slade et al. [17] described a H_2O sub-array that zigzags through the tunnels, with the O atoms centred close to the 8b or 16d sites. In the case of antimonic acid, extra protons are required for charge balance and these bond to either the framework O atoms or form H_3O^+. The 8b and 32e sites in antimonic acid are too close to each other to be both simultaneously occupied by H_2O molecules. Likewise, the cavity centre (8b) and cavity opening (16d) sites are too close to be simultaneously occupied. Consequently, there can only be one H_2O molecule per unit cell present at any one time, although this could be in any of the four possible sites. There have been a number of attempts to locate the water molecules in hydrated defect pyrochlores.

Riviere et al. [18] found that the O of the H_2O molecule in $H_{2x}Sb_{2x}W_{2-2x}O_6 \cdot H_2O$ occupied the 32e site. Dickens and Weller [19] placed the H atoms on the 48f sites and the O and H of the water molecule on the 8b and 32e sites, respectively, in $H_2Ta_2O_6 \cdot xH_2O$. For $DTaWO_6 \cdot D_2O$, Groult et al. [20] placed the deuterons on the 48f sites in a framework of OD groups, with the D and O of the heavy water molecules residing on the 96g and 32e sites, respectively. They surmised that the framework OD is D bonded to the O of the water molecule.

Low-temperature proton NMR studies on $HTaWO_6$ and $HTaWO_6 \cdot H_2O$ by Butler and Biefeld [21], $TaWO_{5.5}$, $HTaWO_6$, $H_2Ta_2O_6$, and $HTaWO_6 \cdot H_2O$ by Groult et al. [20], and $H_2Ta_2O_6$ and $HTaWO_6$ by Durand-Le Floch et al. [22] indicated that the water molecule remains H bonded to the OH framework which demonstrates the absence of H_3O^+ molecules. Slade et al. [17] concluded that three different H atom sites exist in antimonic acid: (1) attached to the framework atoms as hydroxyl groups (H located at 48f and O at 48f), (2) H bonded to framework hydroxyls as H_2O molecules (H located at 8f and O at 32e) and (3) hydrogen bonded to the O atoms at the opening to the cavities as H_3O^+ (H located at 96g and O at 32e).

The general aim of our work is to develop high-quality selective ion-exchange materials based on the pyrochlore structure. This requires that we understand the relationship between the structure and ion-exchange properties. The specific aim of this investigation is to produce a greater understanding of the response of this particular system to temperature. We describe variable temperature structural studies of $NaW_{2-y}Mo_yO_{6+\delta} \cdot nH_{2-z}O$ and report the influence of thermal treatment on the nature of cation/water distribution within the pyrochlore channels, and show the movement of water, but not Na cations, at high temperature.

2. Experimental

2.1. Synthesis

Two pyrochlores with nominal compositions $NaW_2O_6 \cdot nH_2O$ and $NaW_{1.92}Mo_{0.08}O_6 \cdot nH_2O$ (henceforth to be called undoped (U) and doped (D), respectively) were prepared using the hydrothermal method of Reis et al. [23]. For the undoped sample (U), 125 g of 1 M $Na_2WO_4 \cdot 2H_2O$ solution was placed into a 500 ml Teflon container and acidified to a pH of 4.5 with 1 M HCl. The mixture was then heated to 428 K for approximately 30 h in an autoclave. The Mo-doped sample (D) was prepared by adding 174 g of aqueous 1 M $Na_2WO_4 \cdot 2H_2O$ solution to 16.8 g of aqueous 1 M $Na_2MoO_4 \cdot 2H_2O$ solution in a Teflon container and acidifying to a pH of 4.5 with 1 M HCl. The Teflon container was then sealed and placed in an autoclave and heated in an oven at 428 K for 30 h. Upon removal from the oven, the autoclaves were quenched rapidly and the resultant products washed repeatedly with a mixture of ethanol and doubly deionized water. The filtrate was dried overnight at 348 K and then gently ground with an agate mortar and pestle.

2.2. TGA/DTA

Simultaneous thermogravimetric analysis (TGA) and differential thermal analysis (DTA) were performed on a Setaram TAG 24. Approximately 10 mg of each powder was placed in a platinum crucible and heated to 1100 K at a rate of 5 K min^{-1} in flowing air.

2.3. Electron microscopy

The transmission electron microscopy was carried out using a JEOL 2000fxII transmission electron microscope (TEM) operating at 200 kV. The TEM was equipped with a Link super ATW energy dispersive X-ray detector and ISIS microanalysis system. Images and electron diffraction patterns were recorded using a Gatan DualVision 300 W CCD camera attached to the TEM.

2.4. Spectroscopy

IR spectra were collected using a Nexus 8700 FTIR spectrometer fitted with a linearized, liquid N_2-cooled MCT detector. Spectra were measured with a resolution of 4 cm^{-1} by co-addition of 256 scans. Both samples were diluted to 3 wt% in KBr, and the diffuse reflectance measured under a dry air flow of 2 ml min^{-1}, using a Spectra-Tech Collector II accessory equipped with a

high-temperature cell. Spectra were measured over the temperature range of ambient to 673 K in 50-K intervals, and were allowed to equilibrate at temperature for 5 min before collection of each spectrum. Spectra were transformed into Kubelka–Munk units using the spectrum of KBr at each temperature as reference.

^{23}Na magic-angle-spinning (MAS) NMR spectra were acquired at ambient temperature on a Bruker MSL-400 spectrometer (B_0 field of 9.40 T), operating at the ^{23}Na frequency of 105.808 MHz. The ^{23}Na data were acquired using single pulse-acquire (Bloch decay) experiments with a Bruker 4-mm double-air-bearing probe from which MAS frequencies of ~15 kHz were achieved. Non-selective $\pi/2$ pulse times of 2.5 μs were measured on a 1.0 M NaCl solution, from which selective pulse times of ~0.7 μs were employed for data acquisition on all solid samples. Recycle delays of 3 s were typically used, however, the quantification and speciation of these data obtained with these shorter recycle delays were verified with experiments which employed such delays extending to 30 s. All ^{23}Na chemical shifts were referenced to 1.0 M NaCl which was set to δ 0.0 ppm.

2.5. X-ray and neutron diffraction

X-ray diffraction patterns were collected using Cu Kα radiation on a Panalytical X'pert pro diffractometer equipped with an X'celerator high-speed detector and Anton Paar HTK 450 sample cell. Patterns were obtained over the angular range of 5–100° with a step size of 0.0167° and a count time of 25 s per point. Silicon (NIST 640c) was added to each sample in the ratio of 20 wt% Si to sample to act as an internal standard. Lattice parameters were calculated using Jade 7.1. Variable temperature patterns were collected under the following conditions: in 50-K intervals from 83 to 723 K in vacuum at 10^{-7} mbar or 10^{-2} mbar and from 298 to 723 K in air.

Synchrotron X-ray diffraction patterns were recorded on the large Debye–Scherrer diffractometer at the Australian National Beamline Facility (ANBF), Beamline 20B at the Photon Factory, Japan, using 0.79628 Å X-rays [24]. The interior of the large Debye–Scherrer diffractometer was evacuated to 10^{-1} mbar to reduce air scatter of the X-rays. All data were collected on image plates (IP's) and then processed to extract diffraction patterns. Variable temperature data were recorded under a variety of conditions (Table 1) using a custom built furnace.

Sample	Pre-treatment	Environment[a]	Ramp[b]	Soak[c]	Cool[b]
U	Nil	Sealed	373–633 (20)	633, 1 h	613–373 (30)
U	Nil	Sealed	623–1023 (50)	Nil	–
D	Nil	Sealed	373–733 (50)	773, 1 h	–
U	Nil	Unsealed	373–673 (50)	673, 1 h	673–373 (50)
D	Nil	Unsealed	373–673 (50)	673, 1 h	673–373 (50)
U	573 K, 12 h	Sealed	373–673 (50)	673, 1 h	673–423 (50)
D	573 K, 12 h	Sealed	373–673 (50)	673, 1 h	–

[a]Describes if the capillary was sealed or open to atmosphere.
[b]The number in parentheses is the temperature interval.
[c]Time at the highest temperature before cooling the sample.

Powder neutron diffraction data were collected on the medium resolution powder diffractometer (MRPD) instrument ($\lambda = 1.6649$ Å) at the HIFAR facility of the Australian Nuclear Science and Technology Organisation (ANSTO) [25]. Samples were prepared with D_2O in place of H_2O. The U sample was sealed into a vanadium sample can and placed into a closed-cycle cryostat. Powder neutron diffraction profiles were collected at a series of temperatures ranging between 10 and 675 K, and over an angular range of 6–132° in increments of 0.1°.

Structure refinements were carried out by the Rietveld method [26] using the RIETICA program [27] with pseudo-Voigt peak shapes and refined backgrounds for all temperatures.

Table 1
Structural parameters obtained from the Rietveld refinement using the neutron diffraction data for $Na_xW_2O_6 \cdot nH_2O$ at room temperature and at 10 K

Atom	Site	x	$y = z$	B_{iso}	N
W	16c	0	0	4.9(3)	0.0833
Na	16d	0.5	0.5	1.8(8)	0.035(1)
O(1) 10 K	48f	0.3145(3)	0.125	4.5(1)	0.25
O(1) 300 K	48f	0.3146(3)	0.125	5.5(1)	0.25
O(2) 10 K	32e	0.393(2)	0.393(2)	1.8(5)	0.041(3)
O(2) 300 K	32e	0.387(4)	0.387(4)	2.4(5)	0.038(3)
H(1)	48f	0.521(3)	0.125	5.5	0.067(4)

The space group is $Fd\bar{3}m$. N is the site occupancy factor. The displacement parameter of the H/D atoms was constrained to be equal to that of the oxygen atom.

3. Results and discussion

3.1. Characterization

TGA measurements of the undoped sample, U, revealed (Fig. 1) a weight loss of ~5% by 673 K. A broad continuous weight loss from room temperature, corresponding to a weakly bonded (and presumably non-structural) component, is observed together with a more rapid loss near 523 K corresponding to the more tightly bound structural water. This loss precedes the three exothermic events, which are possible phase changes, at 680, 727 and 858 K and two endothermic events at 1009 and 1085 K.

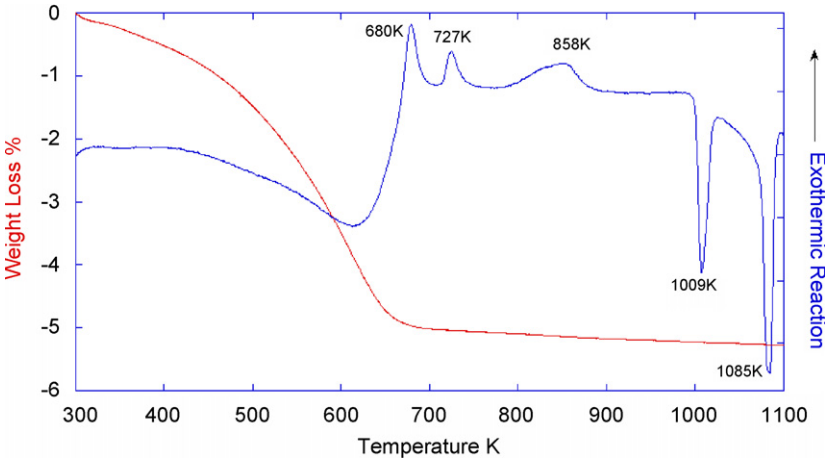

Fig. 1. Simultaneous thermogravimetric analysis of sample $NaW_2O_6 \cdot nH_2O$ acquired from 300 to 1100 K. Note the absence of any phase transition associated with the loss of water at temperatures below 675 K.

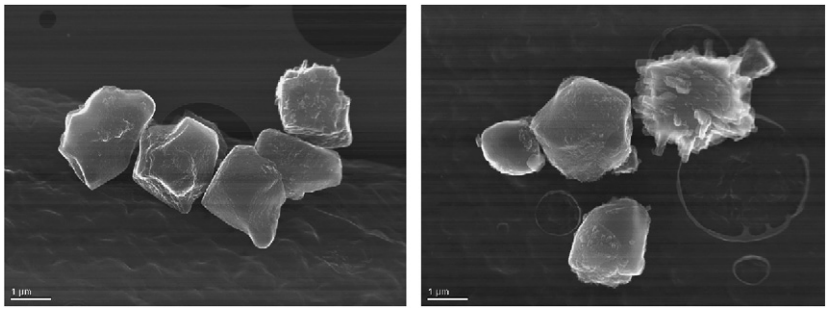

Fig. 2. Scanning transmission electron microscope images of typical unfaceted crystallites, sample $NaW_2O_6 \cdot nH_2O$ and Na $W_{1.92}Mo_{0.08}O_6 \cdot nH_2O$, respectively.

The endothermic events are associated with decomposition and are not discussed further. Similar results were obtained for the Mo-doped sample, D, with features at 679, 725, 827, 1002, 1074 K. These results indicate that water is lost and phase changes occur for both samples at similar temperatures.

Fig. 2 shows TEM images of the typical, unfaceted, grains of sample U and sample D. All grains were about 2–4 μm in size with relatively smooth surfaces, though slight decoration was observed for some grains of sample D. The decoration on sample D could possibly influence the ion-exchange properties of the sample due to an increase in effective surface area. Chemical compositions measured using analytical microscopy were in good agreement with the nominal compositions, the apparent stoichiometry for samples U and D being $Na_{0.99(4)}W_{2.00}O_{6.45}$ and $Na_{1.07(8)}W_{1.97(2)}Mo_{0.03(1)}O_{6.55}$, respectively.

The temperature dependence of the IR spectra for samples U and D on heating to 723 K was very similar, suggesting that doping with Mo had little effect on the structure. The amount of water present in the samples at various temperatures was estimated from the intensity of the deformation band of water at 1625 cm^{-1} and stretching bands at ~3550 and 3500 cm^{-1}.

Fig. 3 shows the change in the 1625 cm^{-1} water deformation band with temperature. The reason for the slight intensity increase on heating to 423 K is not immediately obvious but is presumably related to the loss of physisorbed water. The rapid loss of intensity on heating above this temperature shows that both samples begin to

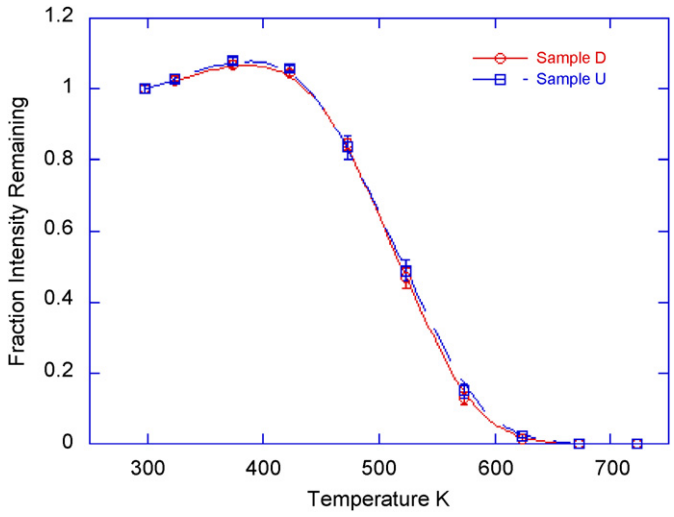

Fig. 3. Temperature dependence of the intensity of water deformation band at 1625 cm^{-1} in the infrared spectrum of undoped $NaW_2O_6 \cdot nH_2O$ and Mo-doped $NaW_{1.92}Mo_{0.08}O_6 \cdot nH_2O$ pyrochlores. Intensities are normalized to the initial intensity. The lines are a guide to the eye.

lose water above 423 K and at 623 K the majority of the H_2O is removed, in agreement with the DTA/TGA results. Only minor shifts were observed for the tungstate bands $<1000\,cm^{-1}$ on heating to 723 K (not shown here), suggesting that the phase changes observed by DTA/TGA involve only subtle changes in the unit cell.

Conventional 1D ^{23}Na MAS NMR techniques were used to investigate the Na speciation in the undoped $NaW_2O_6 \cdot nH_2O$ (U) and Mo-doped $NaW_{2-y}Mo_yO_6 \cdot nH_2O$ (D) samples. Selected ^{23}Na MAS NMR spectra are presented in Fig. 4. The 1D MAS NMR spectra of the as-synthesized U and D samples show that the Na speciation in the two samples is very similar. These ^{23}Na MAS spectra of U and D are dominated by a broad featureless resonance with an apparent chemical shift of ~ -20 ppm. The appearance of this featureless resonance and the extended tailing to the high field side suggests that a distribution of electric field gradients is contributing significantly to the line width and positioning [28–32]. Some dispersion in the isotropic chemical shift (δ_{iso}) is also expected for this resonance. From the second-order quadrupolar contribution to this ^{23}Na resonance line width, the true location of δ_{iso} is expected to be somewhat downfield of -20 ppm, and such distributions of quadrupolar coupling constants (C_Q) and δ_{iso} values reflect intrinsic short-range disorder in the Na positioning and nearest channel neighbours.

Fig. 4 also indicates that two further minor Na species are also present in the as-synthesized samples. The first species is represented by a resonance with an apparent shift of ~ -5 ppm, while the second species is identified by a much broader resonance which is greatly shifted to $\sim +20$ ppm. It is interesting to note that the -5 ppm resonance exhibits far greater intensity in the D sample in comparison to the U analogue, indicating that occupancy of the second Na environment is enhanced when Mo is incorporated into the structure. The very significant downfield shift and exaggerated line width of the latter resonance suggests that a couple of scenarios may pertain (a) a paramagnetic contribution from a residual W(V) component in the structure may be influencing the chemical shift and line broadening mechanism of the resonance associated with this species, or (b) very different solvation effects of the Na^+ channel species may exist involving H_2O, OH^- and combinations thereof. It is interesting to note that the populations of both minor species are profoundly affected by thermal treatments, the intensity of these resonances are greatly diminished by heating to 473 K and both resonances are virtually unobservable after heating to 573 K. The removal of these species upon heating supports the plausibility of both constraints suggested and further work is being undertaken to elucidate the true origins of this speciation phenomenon. From a quantitative perspective, however, these hydration and/or paramagnetic effect(s) pose only a minor perturbation on the total Na channel speciation observed. Indeed, EPR measurements demonstrate the absence of any appreciable amounts of paramagnetic W(V) species.

3.2. Room-temperature structure

The structure of $NaW_2O_6 \cdot nH_2O$ at room temperature was determined using neutron diffraction data (Fig. 5). The structure model was based on that described by Slade et al. [17] for antimonic acid. The atoms of the water molecule were placed at O(2) 32e (x, x, x) and H(1) 48f (x, 1/8, 1/8). Initial refinements were carried out with a fixed x value of 0.3139 for O(1) and 0.4214 for H(1). Only once the refinement had converged was the position and occupancy of the water molecule allowed to vary in the refinements.

It was rapidly established during the refinements that the Na did not fully occupy the 16d sites at (1/2, 1/2, 1/2)

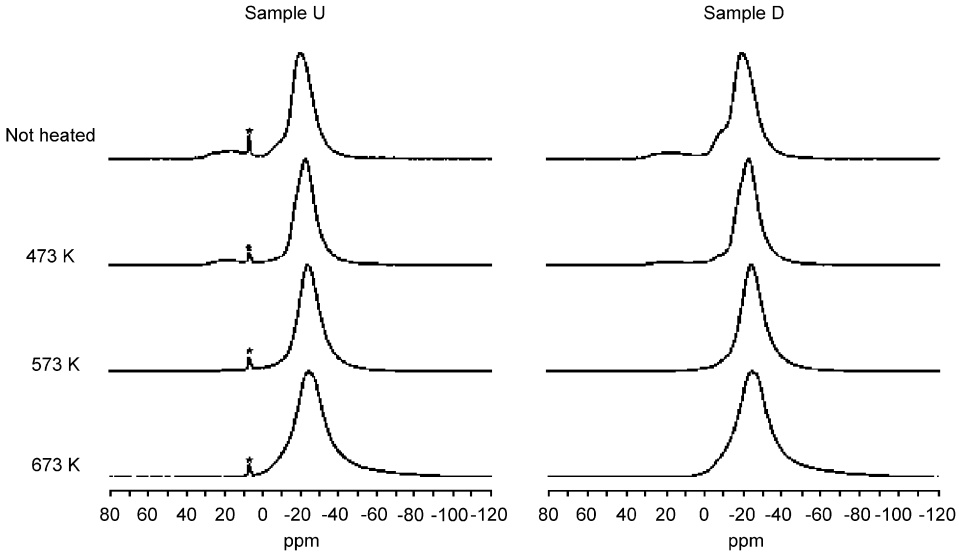

Fig. 4. ^{23}Na MAS NMR spectra of the undoped $NaW_2O_6 \cdot nH_2O$ and Mo-doped $NaW_{1.92}Mo_{0.08}O_6 \cdot nH_2O$ pyrochlores preheated at the temperature indicated for 1 h. The small isotropic resonance at ~7.2 ppm in the U series marked with an asterisk is a minor NaCl contaminant.

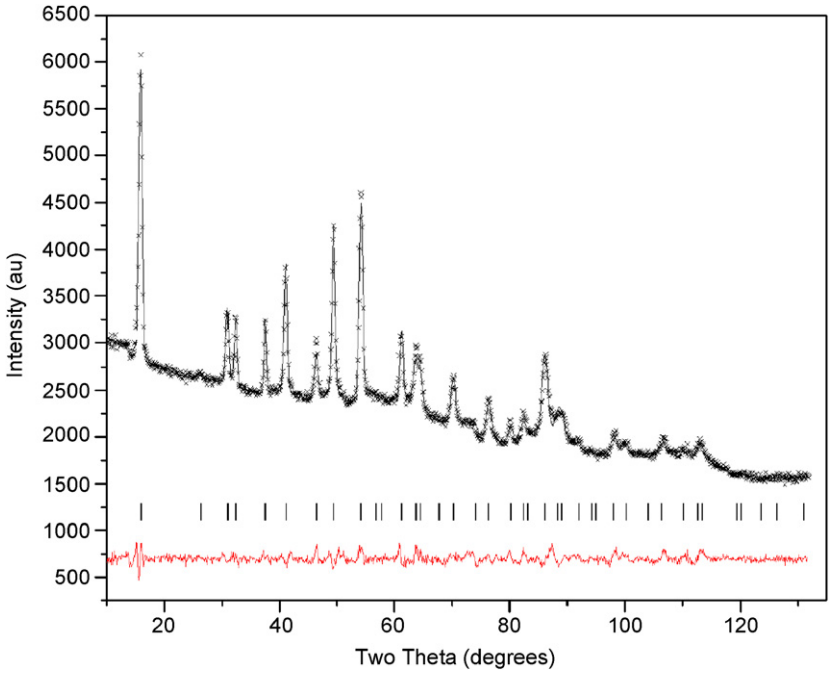

Fig. 5. Neutron diffraction pattern, difference plot and Bragg positions for $NaW_{2-y}Mo_yO_{6+\delta}\cdot nH_{2-z}O$. The larger than expected background is due to incomplete exchange of H_2O with D_2O.

rather the refined occupancy of this site was around 50%. There was no indication from the refinements for any disorder of the Na cations, this being consistent with the lack of obvious streaking in the selected area diffraction pattern. Disorder of the A-site cation is observed in the analogous Cs defect pyrochlores, $CsM_{0.5}W_{1.5}O_6$, M = Ti, Zr, Hf, apparently as a consequence of the large size of the Cs^+ cation [33]. The final measures of fit to the neutron profile were $R_p = 1.77$, $R_{wp} = 2.34$, $R_{exp} = 0.98$, $R_B = 16.21$ and $\chi^2 = 5.65\%$. The value of x for the O(1) site was refined to be 0.3145(3), which shows that there is compression of the octahedra in the [1 1 1] direction. The refined values of x for O(2) and H(1) were 0.393(2) and 0.521(3), respectively.

The W–O(1) distance of 1.947(1) Å is similar to that observed in other W^{VI} oxides and is very similar to the Sb–O distance observed in antimonic acid, 1.974(1) Å, as expected from the similarities in the ionic radii of the two cations W^{VI} and Sb^V, both being given as 0.60 Å [34]. The W–O–W angle is 139.7°(2), which is larger than that observed in antimonic acid, 136.4°. The small but significant differences in the W–O distances and angles of the W_2O_6 framework compared to those in antimonic acid possibly reflect the importance of the channel water molecules.

The structural refinement placed the oxygen atom from the water on a 32e site with $x = 0.393(3)$. The O can be described as being disordered from an 8b site at (3/8, 3/8, 3/8) by displacement of ~0.32 Å in the 111 direction. This site is only partially occupied, the occupancy corresponding to approximately one water molecule per 16d site. As noted earlier, approximately 50% of the 16d sites are vacant and it appears reasonable to suppose that the Na atoms are seven-coordinate, bonding to six O(1) atoms from the W_2O_6 network with Na–O(1) 2.647(2) Å and the one O(2) from the water molecule at 2.06(6) Å. This gives an effective bond valence of the Na ions of 1.1. The H atoms from the water molecule are directed towards the O(1) atoms, although the shortest H–O(1) distance of 2.08(3) Å demonstrates that there is little H-bonding between the water and W_2O_6 framework. The distribution of the Na and water molecules within the channels is illustrated in Fig. 6.

As mentioned earlier, TGA shows the sample loses ~5% of weight when heated to 1100 K. The stoichiometry of the sample based on the Rietveld refinement is $Na_{0.85(2)}W_{2.02(2)}O_6\cdot nH_2O$, $n = 0.92(5)$. The expected weight loss of this composition would be 3.3%, in fair agreement with the observed TGA results. Sorbed water would, of course, be detected in the TGA, but not the neutron diffraction, measurements. This Na:W ratio is in good agreement with the results of X-ray microanalysis that gave a Na:W ratio of 0.99:2. We note that the sample must contain appreciable amounts of hydroxide groups to maintain charge balance, the formula NaW_2O_6 implies a mixed valence W^VW^{VI} composition. NMR and EPR measurements clearly show this not to be the case, rather the stoichiometry is best written as $NaW_2O_6\cdot nH_{2-z}O$. The diffraction data does not provide any evidence for OH^-/H_2O ordering.

In their study of antimonic acid, Slade et al. [17] found two crystallographically unique water molecules. Examination of the Fourier difference maps generated during the structural refinements from the neutron diffraction data

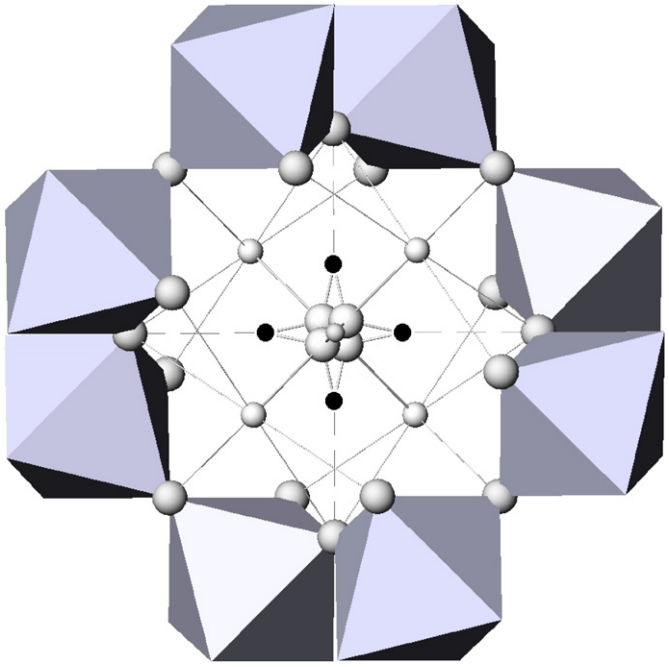

Fig. 6. Representation of $NaW_2O_6 \cdot nH_2O$ structure showing the corner sharing WO_6 octahedra (with O(1) spheres) and the possible locations of O(2), centre spheres with possible hydrogen bonds (- - -) to O(1) located on octahedra vertices and Na situated between both O species in the channels.

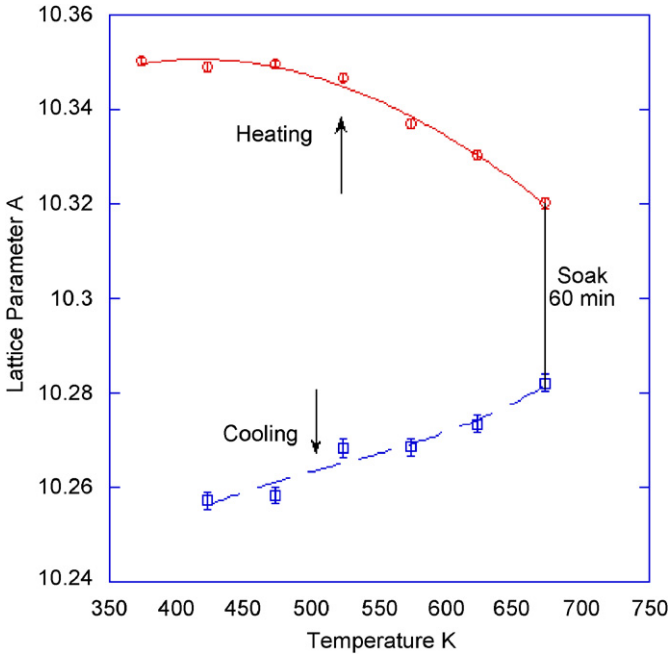

Fig. 7. Temperature dependence of the cubic lattice parameter (synchrotron X-ray) for the $NaW_2O_6 \cdot nH_2O$ recorded in an unsealed capillary. The sample was initially heated to 673 K, held and cooled to 423 K with patterns collected for 10 min at the indicated temperature. The lines are a guide to the eye.

did not reveal evidence for any additional water molecules. Further attempts to place another H_2O molecule in the structure of $NaW_2O_6 \cdot nH_2O$ yielded unstable refinements and we conclude that $NaW_2O_6 \cdot nH_2O$ contains less H_2O than the pyrochlore form of antimonic acid studied by Slade et al.

3.3. Temperature-dependant structural studies

3.3.1. Unsealed system

The lattice parameter of the as-prepared doped and undoped samples was very similar $a \sim 10.35(1)$ Å, with different synthesis giving very slightly different values, possibly as a consequence of small variations in the precise amount of incorporated water. Heating the samples to 573 K for 10 h resulted in a large decrease in the lattice parameter, $a \sim 10.285(3)$ Å. Heating under a dynamic vacuum resulted in a larger reduction in a, heating at 673 K under 10^{-2} mbar reduced a to $\sim 10.28(1)$ Å, and at 673 K under 10^{-7} mbar to 10.24(2) Å. The vacuum presumably assists in the transport of water from the structure. The lattice parameters did not return to their original values immediately but maintained a lattice parameter of $a \sim 10.28(1)$ Å upon standing for several days. This may be due to slow kinetics of water reinsertion. Similar slow kinetics has been observed for the expulsion of water from a pyrochlore structure on reducing pressure [5].

The temperature dependence of the lattice parameters for sample U is illustrated in Fig. 7. This shows a small reduction in the lattice parameter upon heating to 523 K followed by a more dramatic decrease as the temperature increases to 673 K. The contraction upon heating is a consequence of the irreversible loss of water from the sample. The lattice parameter of the resulting dehydrated material is found to show typical behaviour on cooling, that is an approximately linear reduction in a as the temperature is reduced. Sample D showed very similar behaviour. These results are consistent with the TGA and IR results described previously. It was not possible to establish from these X-ray measurements how the mobility of the light Na cations changed either at high temperatures or upon removal of the water.

As a consequence of both the ease of water loss near room temperature and the inability to obtain detailed information on the location of the Na cation and water groups from the XRD studies, variable temperature neutron diffraction studies were also conducted. There are no exotherms or changes in the IR spectra indicative of phase changes below 450 K; therefore, we expect that the only structural variation should be from the position of the water and/or Na ions. The TGA and IR results described previously suggest that little water is lost below 373 K.

The W–O(1) distance and W–O–W angle were remarkably constant between 10 and 625 K with the W–O(1) distance unaltered being 1.949(1) Å at 10 K and 1.947(1) Å at 625 K. Over the same temperature range, the bond angle increased from 139.4(2)° to 140.1(2)°. These structural results are summarized in Table 1.

The temperature dependence of the occupancies for the non-framework atoms Na, O(2), and H(1) is plotted in

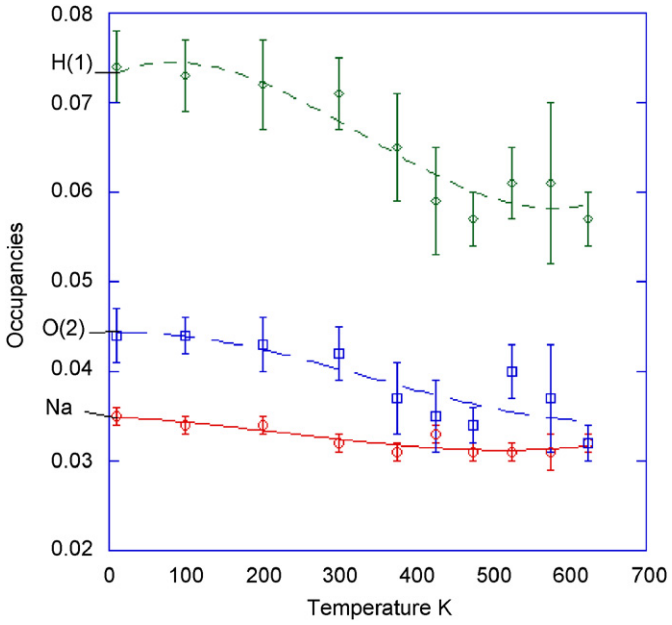

Fig. 8. Temperature dependence of the Na (—), O(2) (– – –) and H(1) (- - - - -) occupancies in $NaW_2O_6 \cdot nH_2O$ obtained from Rietveld refinement of powder neutron diffraction illustrating the more rapid decrease in O(2) and H(1) occupancy compared to the Na occupancy. The lines are a guide to the eye.

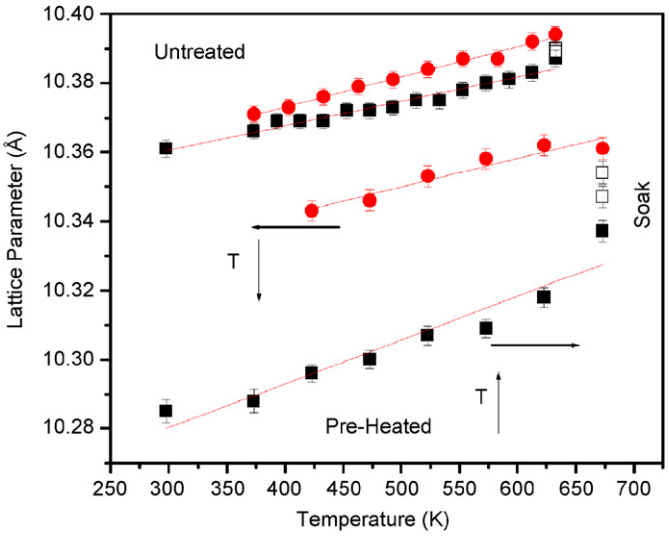

Fig. 9. Thermal expansion of sample U pre-heated to 573 K for 1 h and as-prepared. In both cases, the sample was housed in a sealed capillary. The black squares are data collected with progressively increasing temperature, the open symbols are data collected during a soak at the highest temperature and the circles data collected during cooling. The hysteresis in the thermal expansion is thought to be due to cation migration. The lines are a guide to the eye.

Fig. 8 and illustrates the loss of H_2O from the structure. Whereas the Na content remains reasonably constant, the occupancies of O(2) and H(1) decrease slightly between 300 and 600 K due to the loss of water with a more dramatic loss observed above 660 K.

3.3.2. *Sealed system*

Synchrotron X-ray diffraction measurements were also performed on samples sealed in quartz capillaries to prevent the water from escaping. The temperature dependence of a for the undoped sample is shown in Fig. 9. The thermal expansion of this material is described by the coefficient:

$$\alpha_T = \frac{a_{633} - a_{298}}{a_{298}} = \frac{10.387 - 10.361}{10.361} = 2.51(4) \times 10^{-3}.$$

A small hysteresis is observed upon cooling possibly indicating small changes in the channel occupancies. The neutron diffraction measurements suggest that the sodium cations do not move during heating of the hydrated sample, suggesting the very small irreversibility is due to the rearrangement of the water within the channels. The thermal expansion of the same material preheated to 573 K before sealing the capillary is slightly larger:

$$\alpha_T = \frac{a_{633} - a_{298}}{a_{298}} = \frac{10.337 - 10.285}{10.285} = 5.06(3) \times 10^{-3}.$$

That water was completely removed from this sample is unequivocally demonstrated by the lattice parameter at room temperature being ~10.28 Å, which is close to that observed as the final value on dehydration of the hydrated material. Very similar results were obtained for the analogous Mo-doped samples.

A large hysteresis is observed in the thermal expansion properties of the pre-dried sample, with the cubic lattice parameter and hence volume continuing to expand upon holding at elevated temperatures. This is unexpected and is clearly not related to the presence of water. The continued expansion of the lattice parameter suggests that the structure of the dehydrated material is altered by thermal treatment. Two possible causes of this are disorder of the Na^+ cations from the 16d sites or chemical reduction of the pyrochlore. The absence of any noticeable colour change in the sample after thermal annealing strongly argues against the latter explanation. The relatively poor X-ray scattering power of Na^+ with respect to W_2O_6 precludes us from confirming that displacement of the Na^+ cations occurs in the dehydrated material, nevertheless this is the most feasible explanation for the observed behaviour. The gradual change in the lattice parameter in the soak stage of the experiments may be a consequence of the slow kinetics mentioned earlier, and is analogous to the results reported by Barnes et al. [5]. If the change in the lattice parameter reflects the rearrangement of the A-type Na cations within the channels of the pyrochlore structure, these results demonstrate the rate of rearrangement to be relatively slow and most critically to be strongly influenced by the presence or absence of water in the channels.

4. Summary of conclusions

Powder neutron diffraction studies of the hydrated pyrochlore $NaW_2O_6 \cdot nH_2O$, n~0.92 have shown that both

the Na^+ cations and water molecules reside within the channels that form in the 111 direction of the W_2O_6 framework. The water molecule bonds strongly to the Na cations but only weakly interacts with the W_2O_6 framework. The weakness of this interaction suggests that the water molecules may be highly mobile with in the channels and this property is postulated to be important for the ion-exchange properties of these pyrochlores. The structural studies do not offer any obvious reason for the altered ion-exchange properties observed on doping the pyrochlore with small amounts of Mo. Variable temperature TGA, neutron diffraction and infrared measurements all show that the pyrochlore structure remains essentially unaltered during the removal of the channel water molecules. However, thermal analysis suggests that the water molecules are critical for the stability of the pyrochlore structure with the material rapidly decomposing once all the water is removed.

Anomalous thermal expansion in the lattice parameters was observed when the diffraction measurements were performed on samples within sealed quartz capillaries. This appears to be a consequence of the movement of Na^+ cations from the 16d sites in the pyrochlore channels.

Acknowledgements

The synchrotron section of this work was supported by the Australian Synchrotron Research Program (ASRP) proposal 03/04-AB-31. The authors wish to thank Dave Cassidy for performing the DTA/TGA analysis.

References

[1] V. Luca, C.S. Griffith, H. Chronis, J. Widjaja, Mater. Res. Soc. Symp. Proc. 807 (2004).
[2] C.S. Griffith, V. Luca, Chem. Mater. 16 (2004) 4992.
[3] H.R. von Gaertner, Neues Jahrb. Mineral. Geol. Beil.-Bd. 61 (1930) 1.
[4] M.A. Subramanian, G. Aravamudan, G.V.S. Rao, Prog. Solid State Chem. 15 (1983) 55.
[5] P.W. Barnes, P.M. Woodward, Y. Lee, T. Vogt, J.A. Hriljac, J. Am. Chem. Soc. 125 (2003) 4572.
[6] T. Möller, A. Clearfield, R. Harjula, Chem. Mater. 13 (2001) 4767.
[7] T. Möller, R. Harjula, M. Pillinger, A. Dyer, J. Newton, E. Tusa, S. Amin, M. Webb, A. Araya, J. Mater. Chem. 11 (2001) 1526.
[8] T. Möller, R. Harjula, A. Paajanen, Sep. Sci. Technol. 38 (2003) 2995.
[9] T. Möller, R. Harjula, P. Kelokaski, K. Vaaramaa, P. Karhu, J. Lehto, J. Mater. Chem. 13 (2003) 535.
[10] T. Möller, A. Clearfield, R. Harjula, Microporous Mesoporous Mater. 54 (2002) 187.
[11] A.I. Bortun, L.N. Bortun, D.M. Poojary, O. Xiang, A. Clearfield, Chem. Mater. 12 (2000) 294.
[12] V. Luca, J.V. Hanna, M.E. Smith, M. James, D.R.G. Mitchell, J.R. Bartlett, Microporous Mesoporous Mater. 55 (2002) 1.
[13] A. Tripathi, D.G. Medvedev, M. Nyman, A. Clearfield, J. Solid State Chem. 175 (2003) 72.
[14] T. Möller, Academic Dissertation, Faculty of Science, Department of Chemistry, University of Helsinki, 2002.
[15] E.M. Es'kova, I.I. Nazarenko, Tr. Inst. Mineralog., Geokhim. i Kristallokhim. Redkikh Elementov, Akad. Nauk SSSR (1960) 33.
[16] A. Bystrom, Arkiv Kemi, Mineral. Geol. A 18 (1945) 8.
[17] R.C.T. Slade, G.P. Hall, A. Ramanan, E. Prince, Solid State Ionics 92 (1996) 171.
[18] M. Riviere, J.L. Fourquet, J. Grins, M. Nygren, Mater. Res. Bull. 23 (1988) 965.
[19] P.G. Dickens, M.T. Weller, Solid State Commun. 59 (1986) 569.
[20] D. Groult, J. Pannetier, B. Raveau, J. Solid State Chem. 41 (1982) 277.
[21] M.A. Butler, R.M. Biefeld, Phys. Rev. B 19 (1979) 5455.
[22] M. Durand-Le Floch, J. Pannetier, C. Doremieux-Morin, H. Arribart, J. Chem. Phys. 84 (1986) 4760.
[23] K.P. Reis, A. Ramanan, M.S. Whittingham, Chem. Mater. 2 (1990) 219.
[24] T.M. Sabine, B.J. Kennedy, R.F. Garrett, G.J. Foran, D.J. Cookson, J. Appl. Crystallogr. 28 (1995) 513.
[25] S.J. Kennedy, Adv. X-Ray Anal. 38 (1995) 35.
[26] H.M. Rietveld, J Appl. Crystallogr. 2 (1969) 65.
[27] C.J. Howard, B.A. Hunter, A Computer Program for Rietveld Analysis of X-Ray and Neutron Powder Diffraction Patterns, Lucas Heights Research Laboratories, NSW, Australia, 1998, pp. 1–27.
[28] B.L. Phillips, B.L. Kirkpatrick, G.L. Hovis, Phys. Chem. Miner. 16 (1988) 262.
[29] S.C. Kohn, R. Dupree, M.E. Smith, Geochim. Cosmochim. Acta 53 (1989) 2925.
[30] S.C. Kohn, R. Dupree, M.G. Mortuza, C.M.B. Henderson, Am. Mineral. 76 (1991) 309.
[31] G. Kunath, P. Losso, H. Schneider, S. Steuernagel, C. Jager, Solid State Nucl. Magn. Reson. 1 (1992) 261.
[32] G. Kunath-Fandrei, T.J. Bastow, J.S. Hall, C. Jager, M.E. Smith, J. Phys. Chem. B 99 (1995) 15138.
[33] K. Whittle, G. Lumpkin, S. Ashbrook, J. Solid State Chem. 179 (2006) 512.
[34] R.D. Shannon, Acta Crystallogr. A 32 (1976) 751.